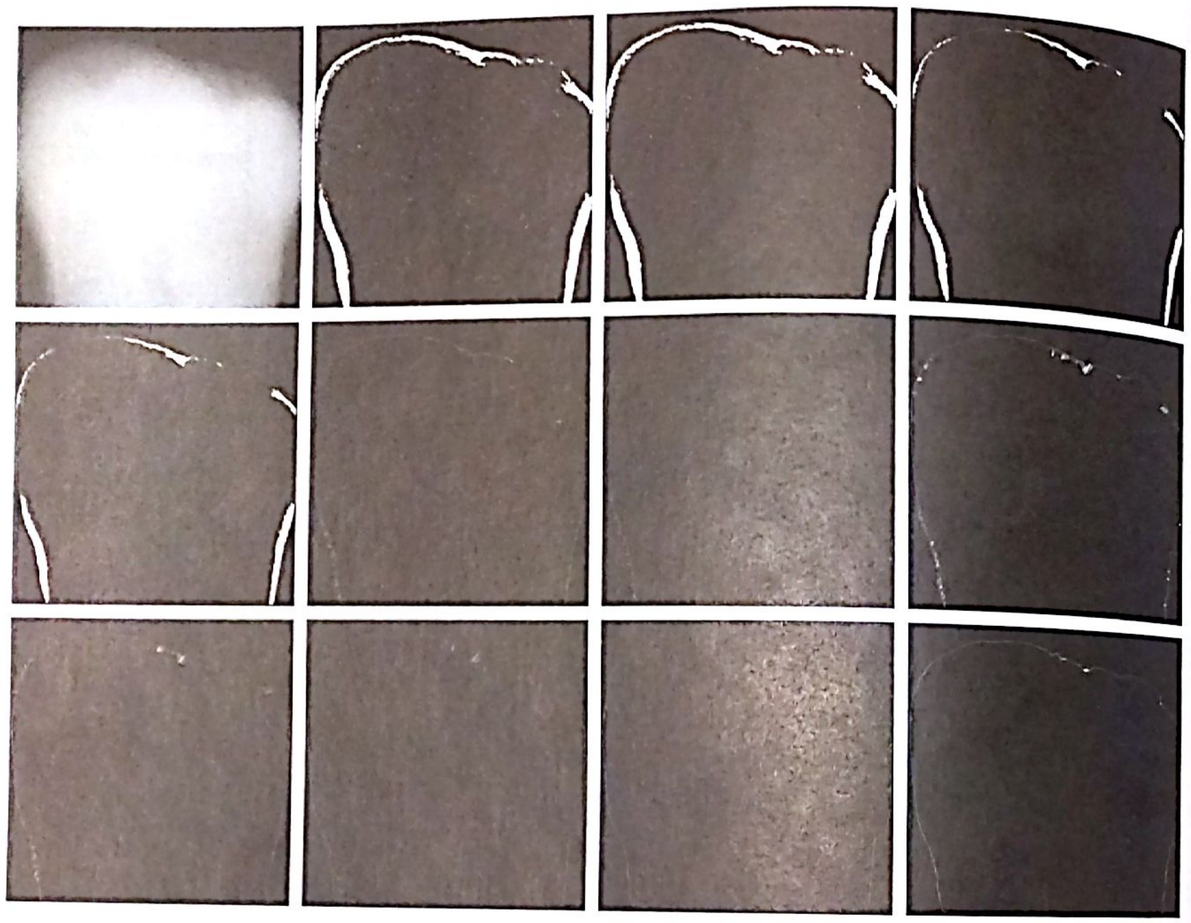

a b c d
e f g h
i j k l

FIGURE 10.30 (a) A 550 × 566 X-ray image of a human tooth. (b) Gradient image. (c) Result of majority filtering. (d) Result of morphological shrinking. (e) Result of morphological cleaning. (f) Skeleton. (g) Spur reduction. (h)–(j) Polygonal fit using thresholds of approximately 0.5%, 1%, and 2% of image width ($T = 3$, 6, and 12). (k) Boundary in (j) smoothed with a 1-D averaging filter of size 1 × 31 (approximately 5% of image width). (l) Boundary in (h) smoothed with the same filter.

required. Figures 10.30(k) and (l) show the result of convolving a 1-D averaging mask with the boundaries in (j) and (h), respectively. The mask used was a 1 × 31 array of 1s, corresponding approximately to 5% of the image width. As expected, the result in Fig. 10.30(k) again is marginal in terms of preserving important shape features (e.g., the right side is severely distorted). On the other hand, the result in Fig. 10.30(l) shows significant boundary smoothing and reasonable preservation of shape features. For example, the roundness of the left-upper cusp and the details of the right-upper cusp were preserved with reasonable fidelity. ■

The results in the preceding example are typical of what can be achieved with the polygon fitting algorithm discussed in this section. The advantage of this

algorithm is that it is simple to implement and yields results that generally are quite acceptable. In Section 11.1.3, we discuss a more sophisticated procedure capable of yielding closer fits by computing minimum-perimeter polygons.

Global processing using the Hough transform

The methods discussed in the previous two sections are applicable in situations where knowledge about pixels belonging to individual objects is at least partially available. For example, in regional processing, it makes sense to link a given set of pixels only if we know that they are part of the boundary of a meaningful region. Often, we have to work with unstructured environments in which all we have is an edge image and no knowledge about where objects of interest might be. In such situations, all pixels are candidates for linking and thus have to be accepted or eliminated based on predefined *global* properties. In this section, we develop an approach based on whether sets of pixels lie on curves of a specified shape. Once detected, these curves form the edges or region boundaries of interest.

Given n points in an image, suppose that we want to find subsets of these points that lie on straight lines. One possible solution is to find first all lines determined by every pair of points and then find all subsets of points that are close to particular lines. This approach involves finding $n(n-1)/2 \sim n^2$ lines and then performing $(n)(n(n-1))/2 \sim n^3$ comparisons of every point to all lines. This is a computationally prohibitive task in all but the most trivial applications.

Hough [1962] proposed an alternative approach, commonly referred to as the *Hough transform*. Consider a point (x_i, y_i) in the xy-plane and the general equation of a straight line in slope-intercept form, $y_i = ax_i + b$. Infinitely many lines pass through (x_i, y_i), but they all satisfy the equation $y_i = ax_i + b$ for varying values of a and b. However, writing this equation as $b = -x_i a + y_i$ and considering the ab-plane (also called *parameter space*) yields the equation of a *single* line for a fixed pair (x_i, y_i). Furthermore, a second point (x_j, y_j) also has a line in parameter space associated with it, and, unless they are parallel, this line intersects the line associated with (x_i, y_i) at some point (a', b'), where a' is the slope and b' the intercept of the line containing *both* (x_i, y_i) and (x_j, y_j) in the xy-plane. In fact, *all* the points on this line have lines in parameter space that intersect at (a', b'). Figure 10.31 illustrates these concepts.

In principle, the parameter-space lines corresponding to all points (x_k, y_k) in the xy-plane could be plotted, and the principal lines in that plane could be found by identifying points in parameter space where large numbers of parameter-space lines intersect. A practical difficulty with this approach, however, is that a

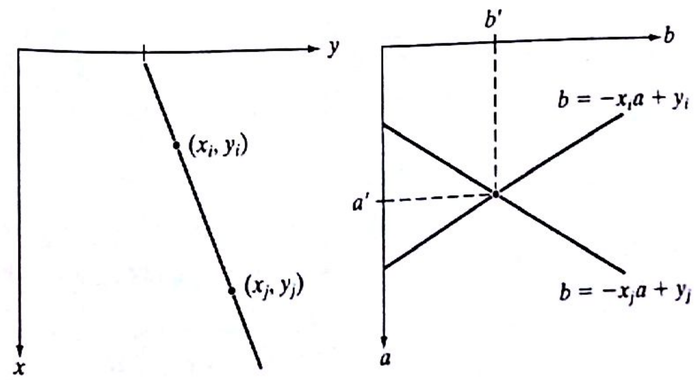

a b

FIGURE 10.31 (a) xy-plane. (b) Parameter space.

(the slope of a line) approaches infinity as the line approaches the vertical direction. One way around this difficulty is to use the normal representation of a line:

$$x \cos\theta + y \sin\theta = \rho \tag{10.2-38}$$

Figure 10.32(a) illustrates the geometrical interpretation of the parameters ρ and θ. A horizontal line has $\theta = 0°$, with ρ being equal to the positive x-intercept. Similarly, a vertical line has $\theta = 90°$, with ρ being equal to the positive y-intercept, or $\theta = -90°$, with ρ being equal to the negative y-intercept. Each sinusoidal curve in Figure 10.32(b) represents the family of lines that pass through a particular point (x_k, y_k) in the xy-plane. The intersection point (ρ', θ') in Fig. 10.32(b) corresponds to the line that passes through both (x_i, y_i) and (x_j, y_j) in Fig. 10.32(a).

The computational attractiveness of the Hough transform arises from subdividing the $\rho\theta$ parameter space into so-called *accumulator cells*, as Fig. 10.32(c) illustrates, where $(\rho_{\min}, \rho_{\max})$ and $(\theta_{\min}, \theta_{\max})$ are the expected ranges of the parameter values: $-90° \le \theta \le 90°$ and $-D \le \rho \le D$, where D is the maximum distance between opposite corners in an image. The cell at coordinates (i, j), with accumulator value $A(i, j)$, corresponds to the square associated with parameter-space coordinates (ρ_i, θ_j). Initially, these cells are set to zero. Then, for every non-background point (x_k, y_k) in the xy-plane, we let θ equal each of the allowed subdivision values on the θ-axis and solve for the corresponding ρ using the equation $\rho = x_k \cos\theta + y_k \sin\theta$. The resulting ρ values are then rounded off to the nearest allowed cell value along the ρ axis. If a choice of θ_p results in solution ρ_q, then we let $A(p, q) = A(p, q) + 1$. At the end of this procedure, a value of P in $A(i, j)$ means that P points in the xy-plane lie on the line $x \cos\theta_j + y \sin\theta_j = \rho_i$. The number of subdivisions in the $\rho\theta$-plane determines the accuracy of the colinearity of these points. It can be shown (Problem 10.24) that the number of computations in the method just discussed is linear with respect to n, the number of non-background points in the xy-plane.

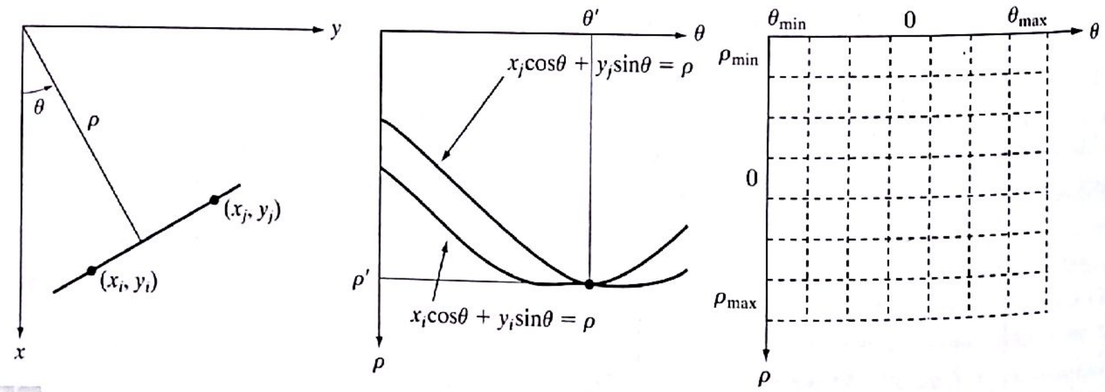

a b c

FIGURE 10.32 (a) (ρ, θ) parameterization of line in the xy-plane. (b) Sinusoidal curves in the $\rho\theta$-plane; the point of intersection (ρ', θ') corresponds to the line passing through points (x_i, y_i) and (x_j, y_j) in the xy-plane. (c) Division of the $\rho\theta$-plane into accumulator cells.

EXAMPLE 10.13: An illustration of basic Hough transform properties.

Figure 10.33 illustrates the Hough transform based on Eq. (10.2-38). Figure 10.33(a) shows an image of size 101×101 pixels with five labeled points, and Fig. 10.33(b) shows each of these points mapped onto the $\rho\theta$-plane using subdivisions of one unit for the ρ and θ axes. The range of θ values is $\pm 90°$, and the range of the ρ axis is $\pm\sqrt{2}D$, where D is the distance between corners in the image. As Fig. 10.33(c) shows, each curve has a different sinusoidal shape. The horizontal line resulting from the mapping of point 1 is a special case of a sinusoid with zero amplitude.

The points labeled A (not to be confused with accumulator values) and B in Fig. 10.33(b) show the colinearity detection property of the Hough transform.

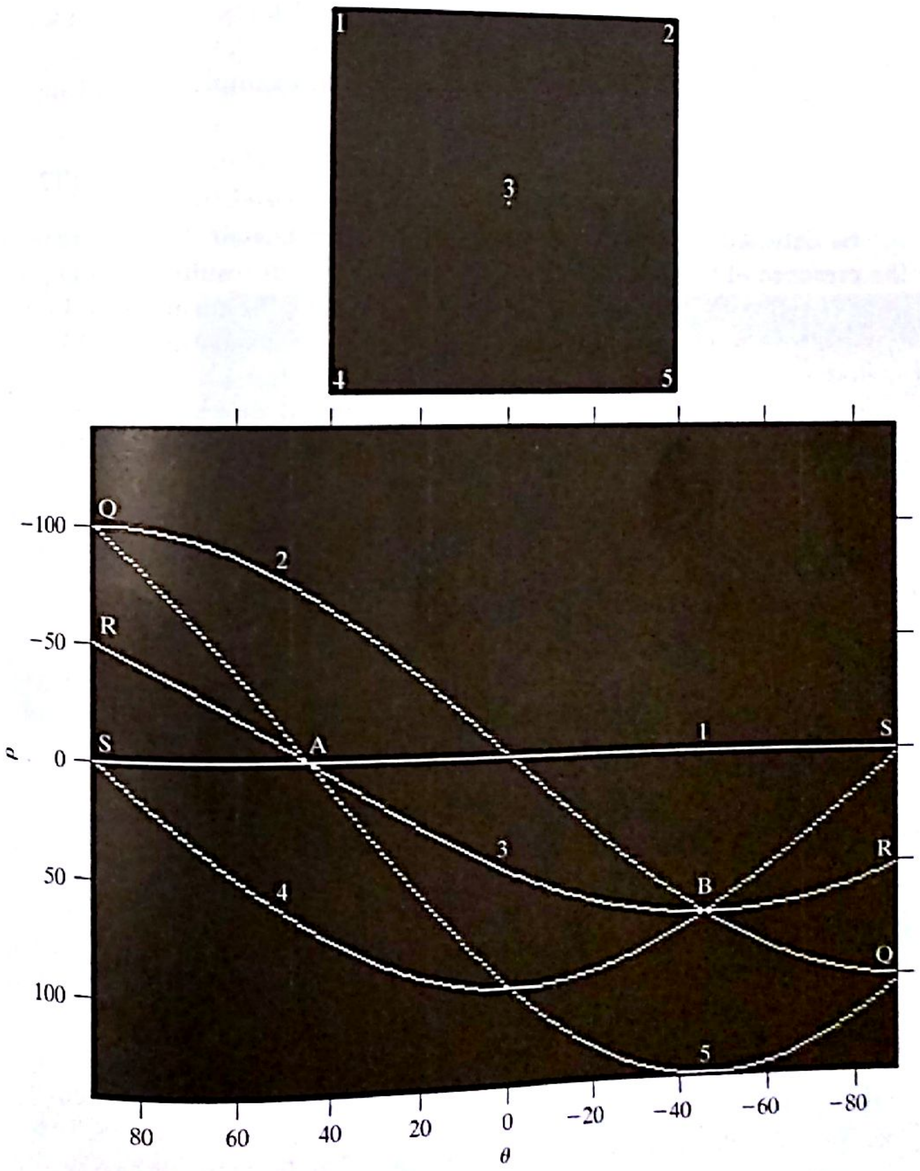

a b

FIGURE 10.33 (a) Image of size 101×101 pixels, containing five points. (b) Corresponding parameter space. (The points in (a) were enlarged to make them easier to see.)

Point A denotes the intersection of the curves corresponding to points 1, 3, and 5 in the xy image plane. The location of point A indicates that these three points lie on a straight line passing through the origin ($\rho = 0$) and oriented at 45° [see Fig. 10.32(a)]. Similarly, the curves intersecting at point B in the parameter space indicate that points 2, 3, and 4 lie on a straight line oriented at −45°, and whose distance from the origin is $\rho = 71$ (one-half the diagonal distance from the origin of the image to the opposite corner, rounded to the nearest integer value). Finally, the points labeled Q, R, and S in Fig. 10.33(b) illustrate the fact that the Hough transform exhibits a reflective adjacency relationship at the right and left edges of the parameter space. This property is the result of the manner in which θ and ρ change sign at the ±90° boundaries. ■

Although the focus thus far has been on straight lines, the Hough transform is applicable to any function of the form $g(\mathbf{v}, \mathbf{c}) = 0$, where $\mathbf{v}$ is a vector of coordinates and $\mathbf{c}$ is a vector of coefficients. For example, points lying on the circle

$$(x - c_1)^2 + (y - c_2)^2 = c_3^2 \qquad (10.2\text{-}39)$$

can be detected by using the basic approach just discussed. The difference is the presence of three parameters (c_1, c_2, and c_3), which results in a 3-D parameter space with cube-like cells and accumulators of the form $A(i, j, k)$. The procedure is to increment c_1 and c_2, solve for the c_3 that satisfies Eq. (10.2-39), and update the accumulator cell associated with the triplet (c_1, c_2, c_3). Clearly, the complexity of the Hough transform depends on the number of coordinates and coefficients in a given functional representation. Further generalizations of the Hough transform to detect curves with no simple analytic representations are possible, as is the application of the transform to gray-scale images. Several references dealing with these extensions are included at the end of this chapter.

We return now to the edge-linking problem. An approach based on the Hough transform is as follows:

1. Obtain a *binary* edge image using any of the techniques discussed earlier in this section.
2. Specify subdivisions in the $\rho\theta$-plane.
3. Examine the counts of the accumulator cells for high pixel concentrations.
4. Examine the relationship (principally for continuity) between pixels in a chosen cell.

Continuity in this case usually is based on computing the distance between disconnected pixels corresponding to a given accumulator cell. A gap in a line associated with a given cell is bridged if the length of the gap is less than a specified threshold. Note that the mere fact of being able to group lines based on direction is a *global* concept applicable over the entire image, requiring only that we examine pixels associated with specific accumulator cells. This is a significant advantage over the methods discussed in the previous two sections. The following example illustrates these concepts.

EXAMPLE 10.14: Using the Hough transform for edge linking.

■ Figure 10.34(a) shows an aerial image of an airport. The objective of this example is to use the Hough transform to extract the two edges of the principal runway. A solution to such a problem might be of interest, for instance, in applications involving autonomous navigation of air vehicles.

The first step is to obtain an edge image. Figure 10.34(b) shows the edge image obtained using Canny's algorithm with the same parameters and procedure used in Example 10.9. For the purpose of computing the Hough transform, similar results can be obtained using any of the edge-detection techniques discussed in Sections 10.2.5 or 10.2.6. Figure 10.34(c) shows the Hough parameter space obtained using 1° increments for θ and 1 pixel increments for ρ.

The runway of interest is oriented approximately 1° off the north direction, so we select the cells corresponding to ±90° and containing the highest count because the runways are the longest lines oriented in these directions. The small white boxes on the edges of Fig. 10.34(c) highlight these cells. As mentioned earlier in connection with Fig. 10.33(b), the Hough transform exhibits adjacency at the edges. Another way of interpreting this property is that a line oriented at +90° and a line oriented at −90° are equivalent (i.e., they are both vertical). Figure 10.34(d) shows the lines corresponding to the two accumulator cells just discussed, and Fig. 10.34(e) shows the lines superimposed on the

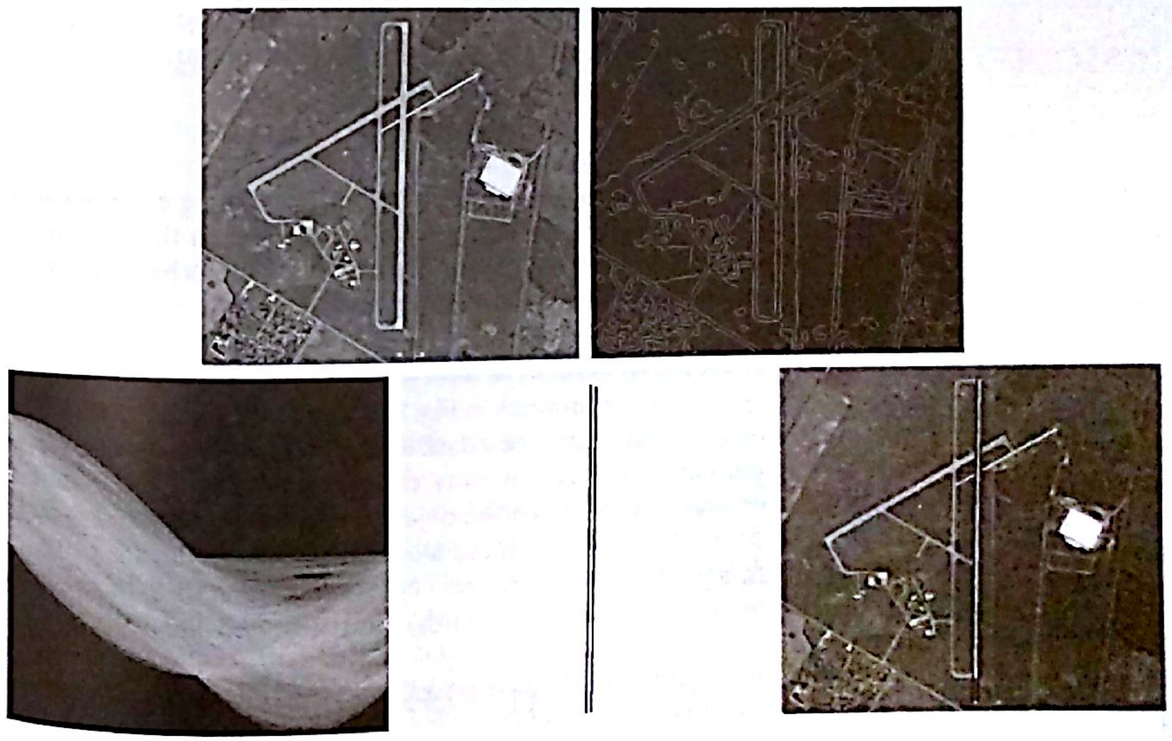

a b
c d e

FIGURE 10.34 (a) A 502 × 564 aerial image of an airport. (b) Edge image obtained using Canny's algorithm. (c) Hough parameter space (the boxes highlight the points associated with long vertical lines). (d) Lines in the image plane corresponding to the points highlighted by the boxes). (e) Lines superimposed on the original image.

original image. The lines were obtained by joining all gaps not exceeding 20% of the image height (approximately 100 pixels). These lines clearly correspond to the edges of the runway of interest.

Note that the only key knowledge needed to solve this problem was the orientation of the runway and the observer's position relative to it. In other words, a vehicle navigating autonomously would know that if the runway of interest faces north, and the vehicle's direction of travel also is north, the runway should appear vertically in the image. Other relative orientations are handled in a similar manner. The orientations of runways throughout the world are available in flight charts, and direction of travel is easily obtainable using GPS (Global Positioning System) information. This information also could be used to compute the distance between the vehicle and the runway, thus allowing estimates of parameters such as expected length of lines relative to image size, as we did in this example. ■

10.3 Thresholding

Because of its intuitive properties, simplicity of implementation, and computational speed, image thresholding enjoys a central position in applications of image segmentation. Thresholding was introduced in Section 3.1.1, and we have used it in various discussions since then. In this section, we discuss thresholding in a more formal way and develop techniques that are considerably more general than what has been presented thus far.

10.3.1 Foundation

In the previous section, regions were identified by first finding edge segments and then attempting to link the segments into boundaries. In this section, we discuss techniques for partitioning images directly into regions based on intensity values and/or properties of these values.

The basics of intensity thresholding

Suppose that the intensity histogram in Fig. 10.35(a) corresponds to an image, $f(x, y)$, composed of light objects on a dark background, in such a way that object and background pixels have intensity values grouped into two dominant modes. One obvious way to extract the objects from the background is to select a threshold, T, that separates these modes. Then, any point (x, y) in the image at which $f(x, y) > T$ is called an *object point*; otherwise, the point is called a *background point*. In other words, the segmented image, $g(x, y)$, is given by

$$g(x, y) = \begin{cases} 1 & \text{if } f(x, y) > T \\ 0 & \text{if } f(x, y) \leq T \end{cases} \qquad (10.3\text{-}1)$$

Although we follow convention in using 0 intensity for the background and 1 for object pixels, any two distinct values can be used in Eq. (10.3-1).

When T is a constant applicable over an entire image, the process given in this equation is referred to as *global thresholding*. When the value of T changes over an image, we use the term *variable thresholding*. The term *local* or *regional thresholding* is used sometimes to denote variable thresholding in

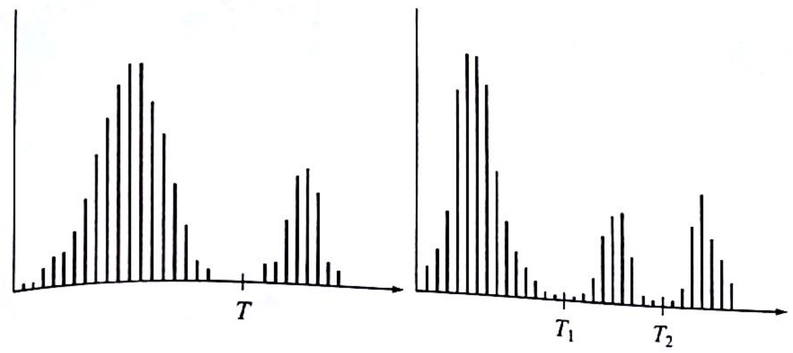

a b

FIGURE 10.35 Intensity histograms that can be partitioned (a) by a single threshold, and (b) by dual thresholds.

which the value of T at any point (x, y) in an image depends on properties of a neighborhood of (x, y) (for example, the average intensity of the pixels in the neighborhood). If T depends on the spatial coordinates (x, y) themselves, then variable thresholding is often referred to as *dynamic* or *adaptive* thresholding. Use of these terms is not universal, and one is likely to see them used interchangeably in the literature on image processing.

Figure 10.35(b) shows a more difficult thresholding problem involving a histogram with three dominant modes corresponding, for example, to two types of light objects on a dark background. Here, *multiple thresholding* classifies a point (x, y) as belonging to the background if $f(x, y) \leq T_1$, to one object class if $T_1 < f(x, y) \leq T_2$, and to the other object class if $f(x, y) > T_2$. That is, the segmented image is given by

$$g(x, y) = \begin{cases} a & \text{if } f(x, y) > T_2 \\ b & \text{if } T_1 < f(x, y) \leq T_2 \\ c & \text{if } f(x, y) \leq T_1 \end{cases} \qquad (10.3\text{-}2)$$

where a, b, and c are any three distinct intensity values. We discuss dual thresholding in Section 10.3.6. Segmentation problems requiring more than two thresholds are difficult (often impossible) to solve, and better results usually are obtained using other methods, such as variable thresholding, as discussed in Section 10.3.7, or region growing, as discussed in Section 10.4.

Based on the preceding discussion, we may infer intuitively that the success of intensity thresholding is directly related to the width and depth of the valley(s) separating the histogram modes. In turn, the key factors affecting the properties of the valley(s) are: (1) the separation between peaks (the further apart the peaks are, the better the chances of separating the modes); (2) the noise content in the image (the modes broaden as noise increases); (3) the relative sizes of objects and background; (4) the uniformity of the illumination source; and (5) the uniformity of the reflectance properties of the image.

The role of noise in image thresholding

As an illustration of how noise affects the histogram of an image, consider Fig. 10.36(a). This simple synthetic image is free of noise, so its histogram consists of two "spike" modes, as Fig. 10.36(d) shows. Segmenting this image into two regions is a trivial task involving a threshold placed anywhere between the two